Cell Reports
Physical Science

CellPress
OPEN ACCESS

Article

Management of electroluminescence from silver-doped colloidal quantum well light-emitting diodes

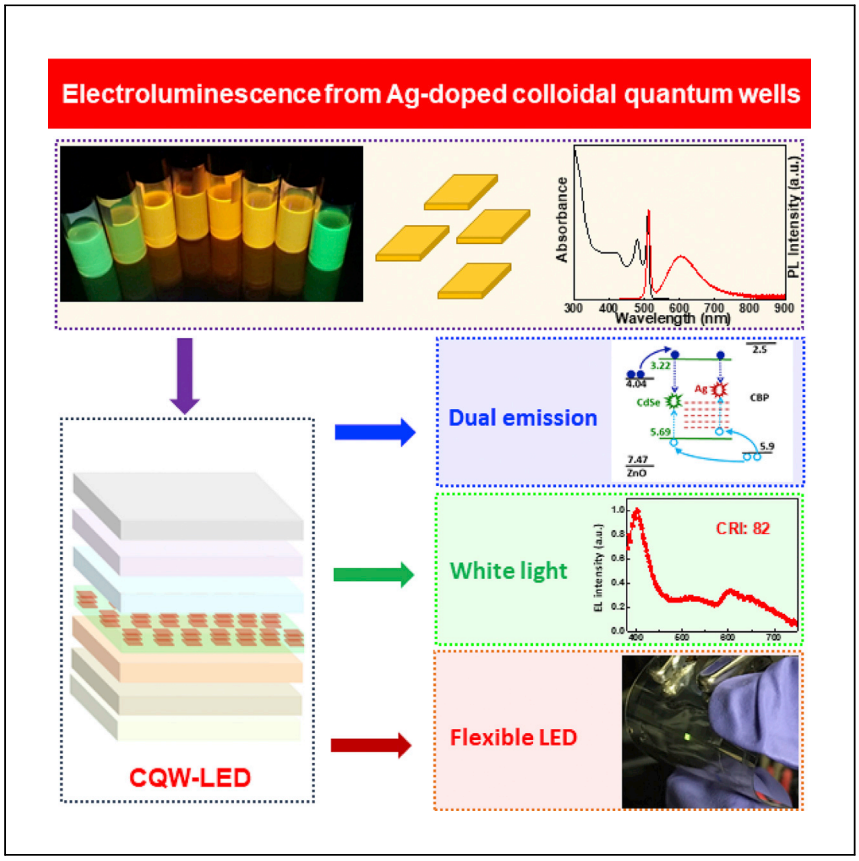

Liu et al. report on electroluminescence from Ag-doped CdSe colloidal quantum wells. Energy gap engineering to manage exciton recombination is a feasible strategy for tunable electroluminescence emission of light-emitting diodes. Organic-inorganic hybrid white light-emitting diodes based on colloidal quantum wells and flexible colloidal quantum well light-emitting diodes are reported.

Baiquan Liu, Manoj Sharma, Junhong Yu, ..., Cuong Dang, Handong Sun, Hilmi Volkan Demir

hvdemir@ntu.edu.sg

Highlights

Electroluminescence from noble metal-doped nanocrystals

Energy gap engineering to manage exciton recombination and tune emission

Organic-inorganic hybrid white LEDs based on colloidal quantum wells

Flexible colloidal quantum well LEDs

Liu et al., Cell Reports Physical Science 3, 100860
May 18, 2022 © 2022
https://doi.org/10.1016/j.xcrp.2022.100860

Please cite this article in press as: Liu et al., Management of electroluminescence from silver-doped colloidal quantum well light-emitting diodes, Cell Reports Physical Science (2022), https://doi.org/10.1016/j.xcrp.2022.100860

Cell Reports
Physical Science

CellPress
OPEN ACCESS

Article

Management of electroluminescence from silver-doped colloidal quantum well light-emitting diodes

Baiquan Liu,[1,2,9] Manoj Sharma,[2,3,9] Junhong Yu,[2] Lin Wang,[4,5] Sushant Shendre,[2] Ashma Sharma,[2] Merve Izmir,[2,6] Savas Delikanli,[7] Yemliha Altintas,[7,8] Cuong Dang,[2] Handong Sun,[4] and Hilmi Volkan Demir[2,7,10,*]

SUMMARY

Impurity doping is a promising strategy to afford colloidal nanocrystals exhibiting novel optical, catalytic, and electronic characteristics. However, some significant properties of noble metal-doped nanocrystals (NMD-NCs) remain unknown. Here, we report the electroluminescence (EL) from NMD-NCs. By doping silver impurity into cadmium selenide colloidal quantum wells (CQWs), dual-emission emitters are achieved and a light-emitting diode (LED) with a luminance of 1,339 cd m^{-2} is reported. In addition, the proposed energy gap engineering to manage exciton recombination is a feasible scheme for tunable EL emissions (e.g., the dopant emission is tuned from 606 to 761 nm). Furthermore, an organic-inorganic hybrid white LED based on CQWs is realized, reaching a color rendering index of 82. Moreover, flexible CQW-LEDs are reported. The findings present a step to unveil the EL property of NMD-NCs, which can be extended to other noble metal impurities, and pave the pathway for NMD-NCs as a class of electronic materials for EL applications.

INTRODUCTION

Colloidal nanocrystals (NCs) have great potential for optoelectronic applications, including solar cells, lasers, biological labels, and light-emitting diodes (LEDs), due to their size, shape, and composition-dependent emission, photostability, and high photoluminescence quantum yield (PLQY).[1–3] To pursue NCs with new optical, catalytic, and electronic properties, the impurity doping strategy has been proposed (e.g., manganese [Mn], copper [Cu], cobalt [Co], and europium [Eu] doping).[4–6] Impurity doping is a procedure in which impurity atoms or ions of elements (e.g., transition metal, alkali metal, rare earth, and lanthanide impurities) are deliberately incorporated into semiconductor lattices, endowing more charges (i.e., holes for p-type doping, electrons for n-type doping).[7–9] In addition, extra energy states can be introduced with the exploitation of impurities to control the PL emission of NCs by fixing the position and quantity of doping centers or selecting different types of impurities,[10] which broadens the technological applications of NCs in microelectronics and optoelectronics.

In principle, both common metal and noble metal impurities are promising candidates to offer colloidal NCs with new functionalities.[11] Nevertheless, studies of noble metal-doped nanocrystals (NMD-NCs) are limited.[12,13] As a result, some significant properties of NMD-NCs may remain unknown. Because noble metal atoms

[1]School of Electronics and Information Technology, Sun Yat-sen University, Guangzhou 510275, China

[2]Luminous! Centre of Excellence for Semiconductor Lighting and Displays, School of Electrical and Electronic Engineering and School of Physical and Mathematical Sciences, Nanyang Technological University, Singapore 639798, Singapore

[3]ARC Centre of Excellence in Exciton Science, Department of Materials Science and Engineering, Monash University, Clayton Campus, Melbourne, VIC 3800, Australia

[4]Division of Physics and Applied Physics, School of Physical and Mathematical Sciences, Nanyang Technological University, Singapore 637371, Singapore

[5]Key Laboratory of Advanced Display and System Applications of Ministry of Education, Shanghai University, 149 Yanchang Road, Shanghai 200072, China

[6]School of Materials Science and Engineering, Nanyang Technological University, Singapore 639798, Singapore

[7]Department of Electrical and Electronics Engineering, Department of Physics, UNAM-Institute of Materials Science and Nanotechnology, Bilkent University, Ankara 06800, Turkey

[8]Department of Material Science and Nanotechnology Engineering, Abdullah Gul University, Kayseri 38080, Turkey

[9]These authors contributed equally

[10]Lead contact

*Correspondence: hvdemir@ntu.edu.sg

https://doi.org/10.1016/j.xcrp.2022.100860

enable unique properties, including high catalytic activity and selectivity,[14] excellent diffusions even at room temperature,[15] and surprisingly large optical windows,[16] the unexplored characteristics will inevitably restrict the further development of NMD-NCs.[17] As is known, the electroluminescence (EL) property is essential to guarantee the emergence of various types of NC-based LEDs.[18–20] Over the last few years, the investigation of common metal impurity doping sites in NCs as efficient emitters has been booming.[21–23] For example, Janssen et al. reported Cu-related emission in Cu-doped cadmium selenide (CdS) colloidal quantum dots (QDs) by using a forward LED architecture, achieving a maximum luminance of 300 cd m^{-2}.[24] Khan et al. showed the dopant emission from Cu-doped CdS/CdS core/shell QD-LEDs, obtaining a maximum luminance of 280 cd m^{-2}.[25] Hou et al. developed Mn-doped $CsPb(Cl/Br)_3$ perovskite LEDs, attaining a maximum luminance of 389 cd m^{-2}.[26] Despite the fact that the EL property of common metal doped NCs was reported a decade ago,[24] the EL effect of noble metal dopants in NCs has not been unveiled yet, let alone their exploration in LEDs.

Aside from zero-dimensional (0D) QDs, 2D colloidal quantum wells (CQWs), also called semiconductor nanoplatelets, are gaining attention as a novel family of optoelectronic NCs.[27–34] Because CQWs only possess strong quantum confinement in the vertical direction, many unique thickness-dependent optical characteristics have been attained, including extremely narrow spectra, suppressed inhomogeneous emission broadening, giant oscillator strength, and large linear/nonlinear absorption cross-sections.[35–37] To date, some groups,[38–40] including ours,[41–45] have demonstrated that CQWs are highly promising in many optoelectronic fields such as luminescent solar concentrators, lasers, and LEDs. Since 2015, the exploration of impurity-doped CQWs has been thriving.[44] For instance, we demonstrated that Mn-doped CQWs showed magneto-optical properties analogous to those of epitaxially grown quantum wells.[44] Then, we reported that Cu-doped CQWs have great potential for various optoelectronic applications.[45] Based on these facts, it is possible to understand the EL effect of noble metal impurities in NCs via doped CQWs.[46–48] However, CQW-LEDs are promising for display and lighting technologies because they have many excellent advantages, including superior color purity, low voltage, low cost, and high efficiency.[49,50] Some gaps still exist between CQW-LEDs and other types of soft-material LEDs (e.g., organic LEDs, QD-LEDs, perovskite LEDs).[51–54] For example, negligible attention has been paid to the understanding of exciton recombination in CQW-LEDs. In addition, the achievement of high-quality white emission has been a tremendous challenge for CQW-LEDs. Furthermore, flexible CQW-LEDs have not been reported.

In this work, we report, for the first time, the EL effect of noble metal dopants in colloidal NCs. By doping silver (Ag) into CdSe CQWs, dual-emission emitters are obtained. With 0.8% Ag-doped concentration, an LED exhibits a peak luminance of 1,339 cd m^{-2}, which is not only the brightest for NC-based LEDs with impurity emissions but also the brightest among core-only-based CQW-LEDs. By understanding the energy gap engineering, we demonstrate that the management of exciton recombination is an easy and effective scheme to tune the EL emissions (e.g., the dopant emission can be tuned from orange-red 606 nm to near-infrared [NIR] 761 nm). Under electrical injection, Ag-doped CQW-LEDs using different hole transporting layers (HTLs) shows this tunable emission for the same dopant site (i.e., 606–761 nm). This in turn helps us to understand the nature of Ag doping sites and their energy distribution in host CQWs, which is not possible with steady-state optical spectroscopy. In addition, the first organic-inorganic hybrid white LED (WLED) based on CQWs is realized, exhibiting a color rendering index (CRI) of 82, which

Please cite this article in press as: Liu et al., Management of electroluminescence from silver-doped colloidal quantum well light-emitting diodes, Cell Reports Physical Science (2022), https://doi.org/10.1016/j.xcrp.2022.100860

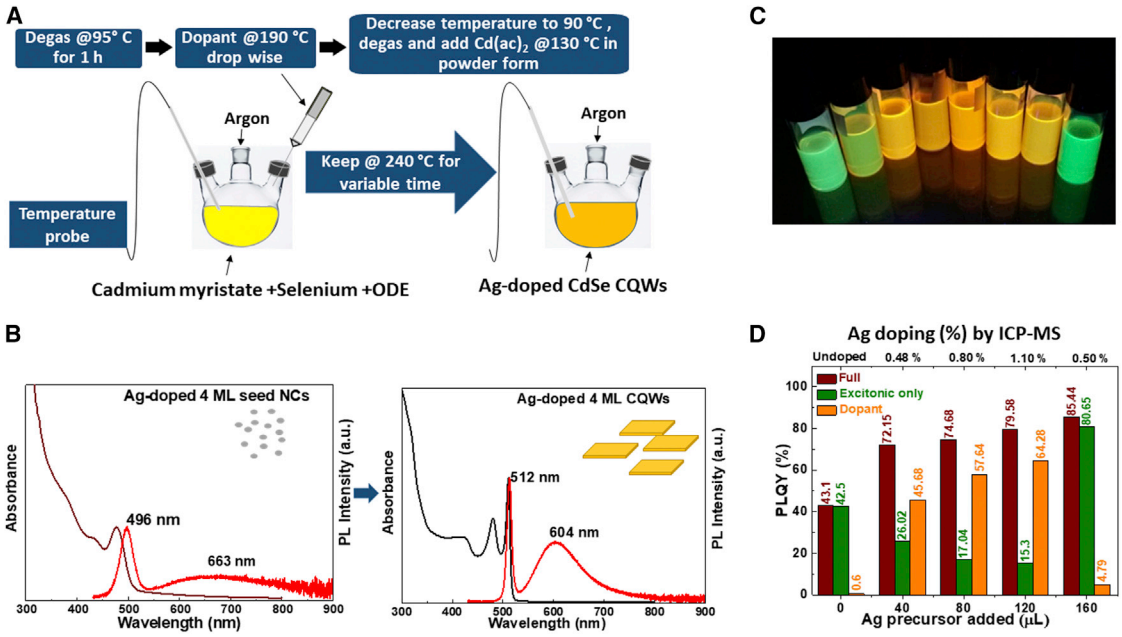

Figure 1. Synthesis and properties of Ag-doped CQWs

(A) Synthesis of Ag-doped CdSe CQWs from CdSe seeds to CQWs.

(B) Absorption and PL spectra of Ag-doped CdSe seeds and CQWs.

(C) Digital pictures of undoped and Ag-doped CdSe CQWs at different Ag concentrations.

(D) PLQY of Ag-doped CQWs with different doping concentrations at excitonic emission and excitonic/dopant emission ranges.

indicates that CQW-based WLEDs can successfully meet the requirement of indoor lighting (i.e., the benchmark CRI is 80). Furthermore, we demonstrate flexible CQW-LEDs, which narrows the gap between CQW-LEDs and other types of state-of-the-art LEDs.

RESULTS AND DISCUSSION

Synthesis and characterization of Ag-doped CQWs

Figure 1A shows the synthesis procedure of Ag-doped CQWs. We mixed a known amount of Cd myristate, Se, and octadecene (ODE) in a round-bottomed flask and degassed it at 95°C for 1 h. After shifting to argon (Ar) and at 190°C, we added a certain amount of Ag dopant precursor, followed by immediate cooling up to 90°C. After again degassing the reaction mixture for 5–10 min, the temperature was set at 240°C, and at 130°C, we added a known amount of Cd acetate powder, which helps in the growth of CQWs from magic-sized nanoclusters. This can be seen in the left part of Figure 1B, where the emission before the addition of Cd acetate is broad for both band emission and dopant-related emission, and the dopant emission is much less than that of the band edge. After adding Cd acetate and keeping the solution at 240°C for the growth of CQWs, we achieved highly efficient Ag^{+}-doped CdSe CQWs. Their absorption and emission spectra of doped seed clusters and corresponding doped CQWs are shown in Figure 1B. Clearly, the excitonic emission at ~513 nm for doped CQWs possesses 10 nm full width at half-maximum (FWHM), which is typical for undoped 4-ML core CdSe CQWs. The FWHM for dopant emission at ~600 nm possesses 98 nm FWHM, which is narrowed with respect to 4-ML seed nanoclusters (~150 nm FWHM). This demonstrates that any contribution coming to dopant emission from small-size polydispersity is reduced strongly after the conversion of seed nanoclusters to strongly confined 2D CQWs, which is unlike

previous Ag-doped CdSe CQWs using the partial cation exchange method with FWHM of Ag-related emissions in the range of 130–150 nm.[47,48]

Figure 1C depicts the varied emissions with varying dopant concentrations as we move from left to right, starting from undoped to highly doped CQWs. After a particular dopant level, the further introduction of dopant ions decreases the dopant emission contribution. To understand this behavior, we showed the PLQY of Ag-doped CQWs with different doping levels shown by the added amount of Ag precursor and actual values of Ag ions in CdSe lattice measured from the inductively coupled plasma-mass spectrometry (ICP-MS) technique (Figure 1D). Undoped CQWs possess the highest PLQY of 43%, while the PLQY of doped CQWs varies from 72% to 85%, with varying contributions from excitonic and dopant emission. With increasing dopant precursor amounts, the actual Ag doping concentration increases. However, after a fixed doping amount, a further increase in dopant precursor decreases actual doping values in host CQWs. We show four different increasing values of added dopant precursor—40, 80, 120, and 160 μL—which results in 0.48%, 0.8%, 1.1%, and 0.5% of Ag doping values with respect to total cations (i.e., Ag and Cd) in the host lattice (Figure 1D). This implies that after 120 μL of dopant precursor, the further addition of dopant ions leads to concentration quenching, and doping values decrease. The overall PLQY remains high at all doping values; however, their contribution among excitonic and dopant emissions shows interesting results. Initially, up to 120 μL of added precursor, the contribution of dopant emission and its related PLQY is increasing, with a constant decrease in emission contribution and PLQY of excitonic emission. Further increases in dopant precursor up to 160 μL result in an increase in PLQY from 79% to 85%. However, the maximum contribution to this high PLQY comes from excitonic emission (up to ~95%). This is interesting because at similar actual doping values (0.48%) the samples show bright yellow emission (with PLQY of 75%) at 40 μL of added precursor. Hence, Ag dopant ions play a different role in both cases. For example, for the samples that show high green excitonic emission, the Ag dopant ions may be adsorbed on surface sites that decrease the nonradiative decay emission, and for the samples that show high dopant emission contribution, the dopant ions may be doped into substitutional sites, leading to efficient Stokes-shifted emission.[55]

EL emission from Ag-doped CQWs

According to the PL spectrum (Figure 1B), Ag-doped CQWs show dual emission (i.e., 512 nm for CdSe excitonic emission and 604 nm for Ag dopant), which makes them promising for lighting, display, nanothermometry, sensing, and integrated photonics.[7–9] As a comparison, undoped CQWs only exhibit CdSe excitonic emission (Figure S1). Despite the fact that Ag impurity has been actively studied,[8] the EL effect of Ag impurity in NCs is unexplored. Furthermore, it is unknown whether dual emission can be achieved under electrical injection, considering the host emission may have disappeared in LEDs.[24]

To reveal the EL effect of NMD-NCs, inverted Ag-doped CQW-LEDs have been developed. As displayed in Figure 2A, the LED configuration is glass/indium tin oxide (ITO)/zinc oxide (ZnO)/CQWs/HTL/MoO_3/Al, where ITO represents the cathode, ZnO represents the electron transporting layer, MoO_3 represents the hole injection layer, and Al represents the anode. With 4,4-*N*,*N*-dicarbazolebiphenyl (CBP) HTL (Figure 2B), devices D1, D2, and D3 have been developed by using CdSe CQWs with 0.48%, 0.8%, and 1.1% Ag-doped concentration as the emitting layer (EML), respectively. The absorption and PL spectra of these three emitters are shown in Figure S2. The high-angle annular dark-field scanning transmission electron microscopy

Please cite this article in press as: Liu et al., Management of electroluminescence from silver-doped colloidal quantum well light-emitting diodes, Cell Reports Physical Science (2022), https://doi.org/10.1016/j.xcrp.2022.100860

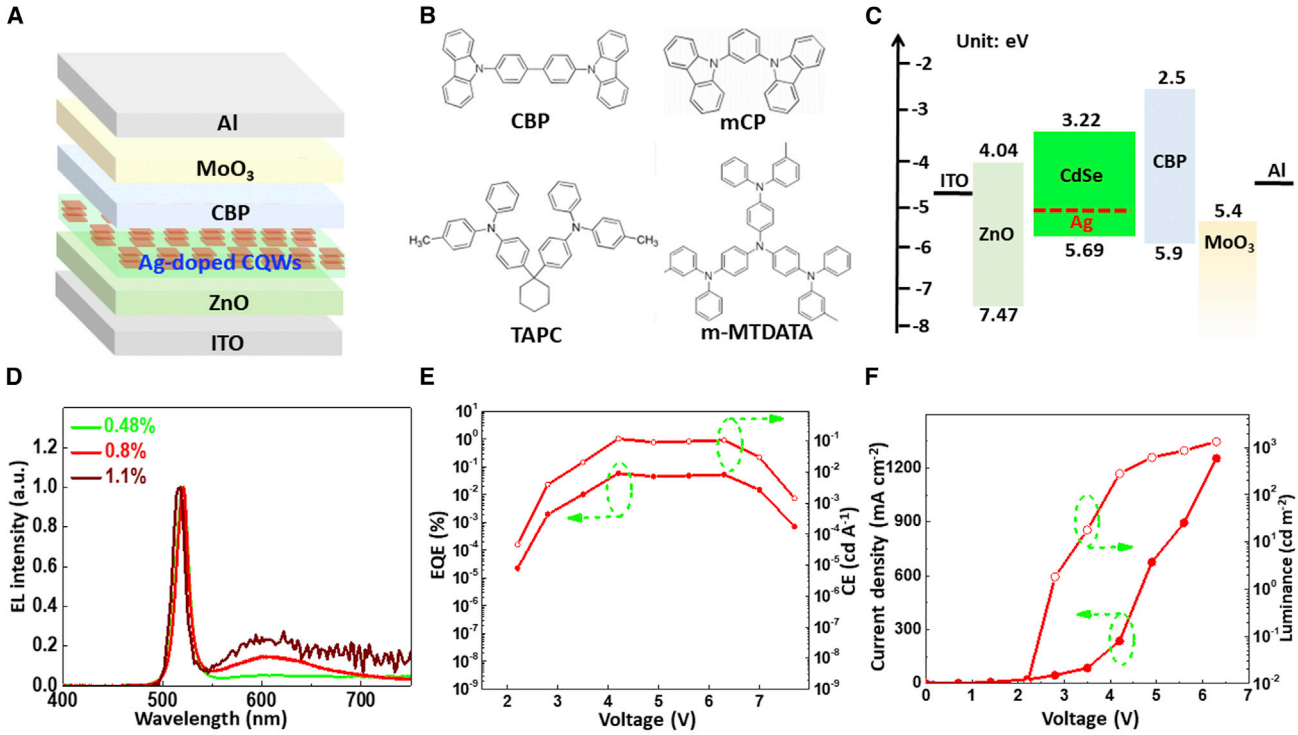

Figure 2. EL effects of Ag-doped CQW-LEDs

(A) Schematic device architecture of CQW-LEDs.

(B) Chemical structures of the hole transporting materials used.

(C) Energy levels of CQW-LEDs. The values are taken from the literature.[4,21,50]

(D) EL spectra of CQW-LEDs at 5 V.

(E) EQE and CE of device D2.

(F) Current density and luminance of device D2.

(HAADF-STEM) images of these three emitters are shown in Figure S3. A cross-sectional scanning electron microscopy (SEM) image of device D2 is shown in Figure S4. In such device architecture, holes and electrons can be efficiently injected into CQWs because of the high hole mobility of CBP (1.0×10^{-3} cm^2 V^{-1} s^{-1}) and high electron mobility of ZnO (1.8×10^{-3} cm^2 V^{-1} s^{-1}) along with the small barrier between the EML and charge transport layers (Figure 2C).[50] As shown in Figure 2D, we have demonstrated that the dual EL emission can be generated by Ag-doped CQWs. Although the Ag doping concentration is only slightly different, the EL spectra of devices D1, D2, and D3 are obviously varied. With the increasing doping concentration, the EL intensity of Ag^+ emission (~608 nm) is increased compared with the intensity of CdSe (~520 nm). This is because more excitons are recombined at the Ag center when a higher doping concentration is used, enhancing Ag^+ emissions. Because device D1 using 0.48% Ag-doped concentration exhibits a weak Ag emission and device D3 with 1.1% Ag-doped concentration shows a poor EL performance (Table 1), we have selected 0.8% Ag-doped CdSe CQWs as the emitter to further understand the EL effect of NMD-NCs.

As shown in Figure 2D and Table 1, the maximum external quantum efficiency (EQE) and current efficiency (CE) of device D2 are 0.059% and 0.118 cd A^{-1}, respectively. Remarkably, the turn-on voltage (the luminance can be detected, $\geq$0.01 cd m^{-2}) is 2.2 V, which is among the lowest LEDs with impurity-doped NCs. Such turn-on voltage is lower than the band gap of CdSe (2.47 eV), which may be attributed to

Table 1. Summary of LED performances

Devices	Emitters[a]	EQE_{max}[b] (%)	CE_{max}[c] (cd A^{-1})	V_{on}[d] (V)	L_{max}[e] (cd m^{-2})
D1	0.48% Ag-doped CQWs	0.042	0.106	2.2	716
D2	0.8% Ag-doped CQWs	0.059	0.118	2.2	1,339
D3	1.1% Ag-doped CQWs	0.045	0.084	2.3	576
W1	PVK: 0.8% Ag-doped CQWs	0.060	0.079	3.0	206
F1	0.8% Ag-doped CQWs	0.086	0.173	2.3	515

[a]Emitters in LEDs.
[b]Maximum EQE.
[c]Maximum CE.
[d]Turn-on voltage.
[e]Maximum luminance.

the sub-band-gap voltage induced by Auger-assisted energy upconversion.[18] Because a high charge density is needed for Auger-assisted charge injection, the sub-band-gap emission may result from electron injection at sub-band-gap voltages. Considering the highest occupied molecular orbital (HOMO) of CBP is deeper than the valance band maximum (VBM) of CdSe, it is barrier free for the hole injection. At low voltages, holes accumulate at the interface of CQWs/ZnO instead of electrons accumulating at the interface of ZnO/CQWs. Hence, conditions for Auger-assisted charge injection may be accomplished at the interface of CQWs/ZnO. Significantly, the maximum luminance is 1,339 cd m^{-2} (Figure 2F). To the best of our knowledge, this value is not only the highest for NC-based LEDs with impurity emissions but also the best among core-only-based CQW-LEDs.

Origin of the EL emission

To understand the origin of the dual EL emission in NMD-NCs, the working mechanism of device D2 has been studied. In device D2, holes transported from CBP are barrier free to be injected into CdSe or trapped by Ag because the HOMO of CBP (5.9 eV) is deeper than the VBM of CdSe and energy level of Ag states.[56] Then, holes meet electrons transported from ZnO at the conduction band minimum (CBM) of CdSe to generate excitons and recombine for CdSe and Ag^+ emissions. Therefore, as shown in Figure 3A, excitons are recombined via two parallel channels (i.e., holes at CdSe VBM and Ag energy states recombined with electrons at CdSe CBM for CdSe and Ag^+ emission, respectively), leading to the dual EL emission. In addition, since Ag possesses several states[21] and all of them are higher than the HOMO of CBP, holes transported from CBP are more likely to reach the low states. Thus, the Ag^+ emission is mainly ascribed to the exciton recombination from electrons at the CdSe CBM, with holes at the low Ag states in device D2. The EL spectra of device D2 at various voltages are shown in Figure 3B, where the intensity of Ag^+ is reduced compared to that of CdSe when the voltage is enhanced. Since Ag energy states are shallower than the HOMO of CBP and VBM of CdSe (5.69 eV), holes are readily trapped by Ag instead of CdSe at low voltages, leading to more excitons recombining for Ag^+ emission.[51] The silver states are not easily saturated, as can be seen in the power-dependent PL study (Figure S5). In addition, the long-lived nature of the Ag emission band (lifetime: ~90 ns) is due to the restricted wavefunction overlap between the Ag-trapped holes and electrons in the CBM of CdSe CQWs.[57] With the enhancing voltage, relatively more holes are injected into the VBM of CdSe. Hence, more excitons can be generated and then recombined for CdSe emission under high voltages.

Due to the existence of various Ag states, holes transported from the HTL can be mainly located at the deliberate states if the energy gap engineering can be

Please cite this article in press as: Liu et al., Management of electroluminescence from silver-doped colloidal quantum well light-emitting diodes, Cell Reports Physical Science (2022), https://doi.org/10.1016/j.xcrp.2022.100860

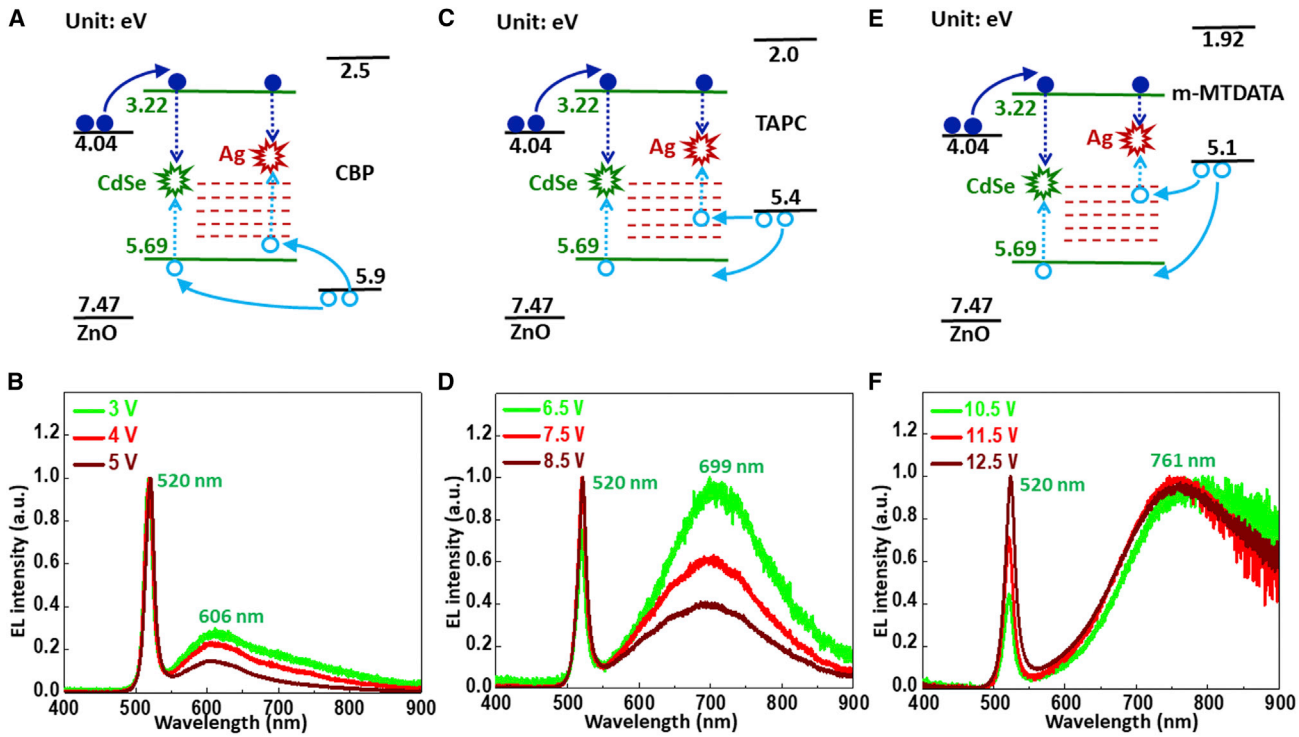

Figure 3. Origin of the tunable EL emissions

(A) Schematic working mechanism of device D2.
(B) EL spectra of device D2 at various voltages.
(C) Schematic working mechanism of device D5.
(D) EL spectra of device D5 at various voltages.
(E) Schematic working mechanism of device D6.
(F) EL spectra of device D6 at various voltages.

managed (e.g., HTLs with appropriate HOMOs are introduced). Therefore, the Ag^+ emission may be tunable, considering that Ag^+ EL emissions originate from the phenomenon that excitons are recombined from holes at Ag states with electrons at the CBM of CdSe. As a result, the Ag^+ emission will be red-shifted if excitons are recombined from holes at the middle or higher Ag states with electrons at CdSe CBM, since the energy gap between CdSe CBM and middle/high Ag states is reduced compared to that between CdSe CBM and lower Ag states. To comprehensively understand the effect of energy gap engineering on the EL of Ag-doped CQWs, several HTLs with suitable HOMOs have been exploited. To further confirm the working mechanism of Ag-doped CQW-LEDs, *N*,*N*′-dicarbazolyl-3,5-benzene (mCP) has been used as the HTL to develop a CQW-LED (device D4) where its device architecture is the same as device D2 except for the HTL (glass/ITO/ZnO/CQWs/mCP/MoO_3/Al). The HOMO of mCP is 6.1 eV,[58] which is even deeper than that of CBP. Thus, the Ag^+ emission peak of device D4 should be the same as that of device D2 because the Ag^+ emission in device D4 is also mainly attributed to the exciton recombination from electrons at CdSe CBM with holes at low Ag states. As expected, the Ag^+ emission peak of 607 nm in device D4 is similar to that of device D2 (Figure S6).

If holes are mainly located at the middle Ag states, the energy gap between the middle Ag states and the CdSe CBM is reduced, which will lead to a red-shifted Ag^+ emission peak. To confirm these assumptions, 1-bis[4-[*N*,*N*-di(4-tolyl)amino]

phenyl]-cyclohexane (TAPC) has been used as the HTL to develop a CQW-LED (device D5) where its device architecture is the same as device D2 except for the HTL (glass/ITO/ZnO/CQWs/TAPC/MoO_3/Al). The HOMO of TAPC is 5.4 eV,[59] which is close to the energy level of the middle Ag states (Figure 3C). Hence, holes transported from TAPC easily reach the middle Ag states and then recombine with electrons at CdSe CBM. As a piece of evidence for these analyses, the EL spectra of device D5 at various voltages have been measured (Figure 3D). As expected, the Ag^+ emission peak in device D5 (~699 nm) is largely red-shifted compared with the spectra of devices D2 and D4. However, the CdSe emission in device D5 (~520 nm) is similar to that of devices D2 and D4. Therefore, by controlling the location of holes at Ag states, the Ag^+ emission can be managed.

Based on the proposed energy gap engineering, it is expected that the Ag^+ emission can be further red-shifted if holes are mainly located at high Ag energy states. To demonstrate this assumption, an HTL with a shallow HOMO is helpful. Toward this end, 4,4′,4″-tris[3-methylphenyl(phenyl)amino]triphenylamine (*m*-MTDATA) has been used as the HTL to develop a CQW-LED (device D6) where its device structure is the same as that of device D2 except for the HTL (glass/ITO/ZnO/CQWs/*m*-MTDATA/MoO_3/Al). The HOMO of *m*-MTDATA is only 5.1 eV, which is shallower than high Ag states.[60] As a result, holes transported from *m*-MTDATA easily reach high Ag states and then recombine with electrons at the CdSe CBM (Figure 3E). As evidence, the Ag^+ emission peak of device F is ~761 nm (Figure 3F), which is remarkably red-shifted compared with that of devices D2, D4, and D5. This NIR emission is mainly attributed to the exciton recombination from the electrons at CdSe CBM, with holes at high Ag states. Hence, only the Ag^+ emission is changed due to the reduced energy gap between Ag states and CdSe CBM, while the CdSe emission peak remains almost the same. With the increasing voltage, holes can reach the VBM of CdSe by overcoming the hole barrier between *m*-MTDATA and CdSe. Therefore, relatively more excitons can be recombined for CdSe emission at high voltages, enhancing the CdSe excitonic emission. Such exciton recommendation is somewhat similar to the exciton decay in the host-guest-system-based organic LEDs (OLEDs), in which charges can be directly injected into the energy levels of guests.[56]

Previously, NCs with low Ag doping concentration could only exhibit red PL emission.[12,46] Here, we have demonstrated that the emission of CQWs with low Ag doping concentration can be tuned from orange-red to the NIR region through energy gap engineering, which may be a unique EL property. In addition, such NIR emission may unlock a new method for the applications of CQW-LEDs, given that NIR emission is beneficial for night vision, optical communication, and medical treatment.[61] Furthermore, we have demonstrated that the management of the energy gap between dopant states and the host CBM is a feasible working mechanism to tune the EL emission. Considering that hole transporting materials can be deliberately synthesized to possess suitable HOMOs,[58] our proposed emission mechanism may be further extended to other host-dopant systems to achieve desirable emissions. Moreover, the large emission window (155 nm) is unprecedentedly reported in NC-based LEDs by using only a single emitter, which may unveil new possibilities for the EL applications of impurity-doped NCs. The performance (e.g., efficiency, stability) of CQW-LEDs may be additionally enhanced, if Ag-doped heterojunction-based CQWs (e.g., Ag-doped CQW core/shell, Ag-doped CQW core/crown), more stable HTLs (e.g., HTLs with high glass transition temperature, HTLs with low electrochemical decomposition, or inorganic HTLs), and the combination of more balanced charge transport layers were used.

Cell Reports
Physical Science
Article

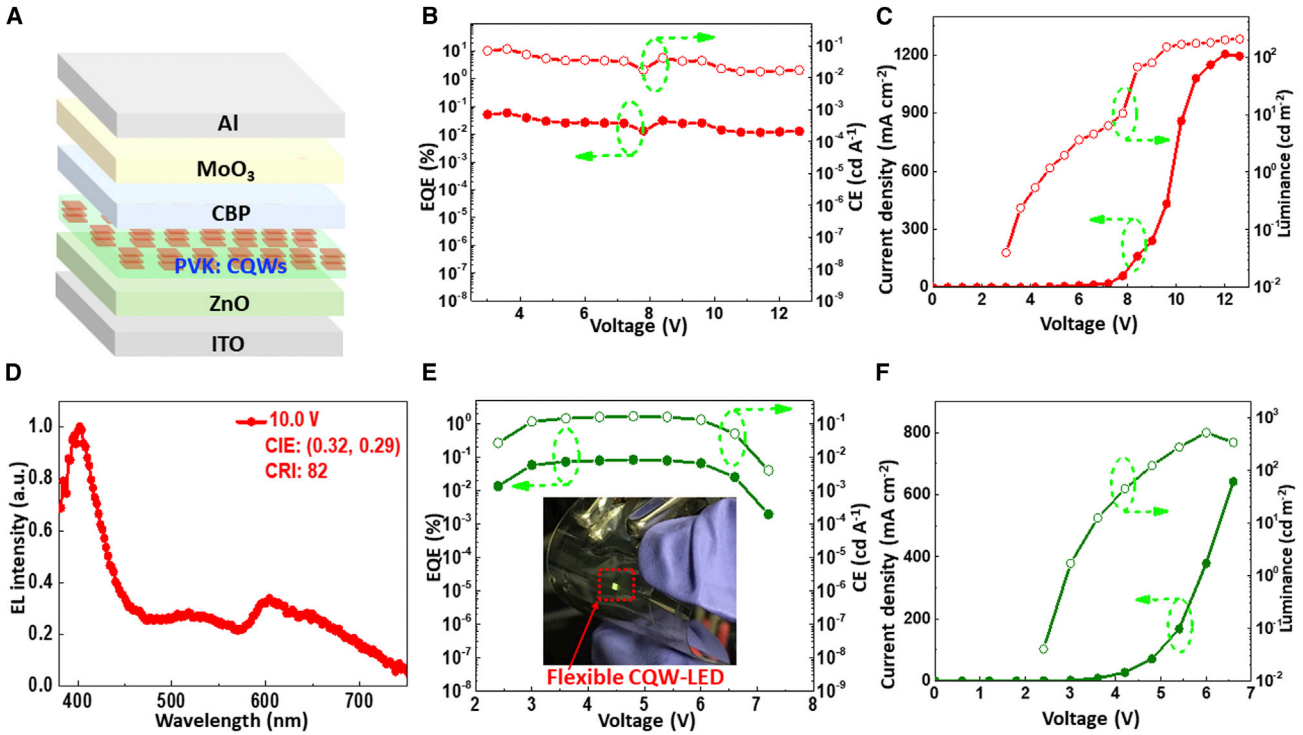

Figure 4. Development of CQW-based WLEDs and flexible devices

(A) Schematic device architecture of WLEDs.

(B) External quantum efficiency (EQE) and current efficiency (CE) of device W1.

(C) Current density and luminance of device W1.

(D) EL spectrum of device W1. The collective voltage is 10.0 V.

(E) EQE and CE of device F. Inset: photograph of device F1 under bias, where the emission area is 1 × 1 mm^2.

(F) Current density and luminance of device F1.

Realization of CQW-based organic-inorganic hybrid WLEDs

WLEDs are highly desirable for both display and lighting applications.[59] In particular, organic-inorganic hybrid WLEDs arouse research interest due to their simple fabrication process, energy-efficient operation, reduced heterojunction, and low cost.[62,63] Several types of NC-based hybrid WLEDs have been created. For example, Gao et al. used QDs and poly-phenylenevinylene (PPV) to fabricate the first CdSe-QD-based hybrid WLED, achieving a maximum EQE of 0.0015%.[62] Recently, Yao et al. used $CsPb(Br/Cl)_3$ and poly[2-methoxy-5-(2-ethylhexyloxy)-1,4-phenylenevinylene] (MEH:PPV) to develop the first perovskite-based hybrid WLED, obtaining a maximum luminance of ≈200 cd m^{-2}.[63] However, no CQW-based organic-inorganic hybrid WLED has been reported thus far. To alleviate this difficulty, we have combined 0.8% Ag-doped CQWs and an organic blue emitter poly(*N*-vinylcarbazole) (PVK) to realize white emissions. The chemical structure, absorption, and PL spectra of PVK are shown in Figure S7, in which a blue PL emission peak of 374 nm is observed. The device architecture of the WLED (device W1) is similar to that of device D2, except for the EML, with an optimized mixing ratio of PVK:CQWs = 6:1 (in wt %) (glass/ITO/ZnO/PVK:CQWs/CBP/MoO_3/Al), as shown in Figure 4A. Device W1 exhibits the maximum EQE and CE of 0.060% and 0.079 cd A^{-1}, respectively (Figure 4B). The maximum power efficiency (PE) is 0.072 lm W^{-1} (Figure S8). In addition, a low turn-on voltage of 3.0 V and a maximum luminance of 206 cd m^{-2} are obtained (Figure 4C). The luminance at 8 V is ~20 cd m^{-2}. The Commission Internationale de L'Eclairage (CIE) coordinates are (0.32,

0.29), which is well located in the white region. Significantly, device W1 shows a maximum CRI of 82 (Figure 4D), indicating that CQW-based WLEDs can successfully meet the requirement of indoor lighting.[64] The CRI values are derived from EL spectra and the analyses are shown in Figure S9.

It is surprising that a high CRI can be achieved by only two emitters since more than two emitters are usually required for high-quality white emissions.[64] To insightfully comprehend CQW-based hybrid WLEDs, the working mechanism of device W1 has been studied. Since PVK is a p-type material while ZnO is an n-type material,[1] holes and electrons are readily accumulated at the PVK/ZnO interface. As a consequence, holes at the HOMO of PVK can recombine with electrons at the CBM of ZnO, generating a PVK/ZnO interface emission.[65] To provide evidence for the interface emission, another LED (device W2) has been fabricated, and its device architecture is similar to device W1, except for the EML, with only PVK (glass/ITO/ZnO/PVK/CBP/MoO_3/Al). With such architecture, only PVK and interface emissions can be produced, while CdSe and Ag^+ emissions are excluded. As expected, apart from the PVK emission (Figure S10), the interface emission is observed with two peaks (606 and 646 nm) in device W2. However, the CIE coordinates of device W2 are (0.54, 0.33) because of the lack of CdSe and Ag^+ emissions, which are beyond the white region. Hence, four emission peaks (402, 518, 604, and 644 nm) exist in the EL spectrum of device W1, where the Ag^+ emission is overlapped with the interface emission. Here, the EL peaks of PVK and excitonic emission of CdSe are located at ~402 and 518 nm. Due to the combination of PVK, CdSe, Ag^+, and PVK/ZnO interface emissions, the broad white emission is achieved in device W1, leading to the high CRI.

In addition, high-energy excitons are transferred from PVK to Ag-doped CdSe through the Förster process because of the large band gap of PVK, where the energy of the excited state of PVK is higher than that of CdSe CQWs.[66] Hence, for the white emissions of device W1, the amount of PVK is six times higher than that of Ag-doped CdSe. To confirm the Förster resonant energy transfer (FRET) existing between PVK and CQWs, we have compared the PL spectrum of PVK with the absorption spectrum of CQWs. These two spectra show a large overlap (Figure S11), suggesting an efficient FRET.[67] Furthermore, the large concentration of CQWs in PVK indicates that the distance between the guest and host is shorter than Förster radius (e.g., typically in the range of 4–7 nm), ensuring the FRET.[68] Therefore, the performance of WLEDs can be further improved if highly efficient blue organic emitters are introduced. However, due to the high amount of PVK in the EML of device W1, PVK has a large influence on the charge injection and balance. Considering that PVK is a p-type emitter, the charge imbalance occurs in device W1, resulting in Auger recombination.[1] Hence, to further enhance the radiative exciton recombination, bipolar organic emitters may be useful to suppress the nonradiative Auger decay. However, these results also indicate that 2D CQWs can effectively work with organic emitters as EMLs to achieve high-quality white emissions, providing an alternative scheme to develop WLEDs.

Demonstration of flexible CQW-LEDs

OLEDs and QD-LEDs have been intensively investigated to satisfy the increasingly flexible electronics market. Recently, flexible perovskite LEDs have also been realized.[69] However, flexible CQW-LED has not been reported. Here, flexible CQW-LEDs have been developed by using polyethylene terephthalate (PET) substrates to replace the glass substrates. Dual-emission emitters have been used to realize flexible device F1, where its device architecture is the same as device D2, except

Please cite this article in press as: Liu et al., Management of electroluminescence from silver-doped colloidal quantum well light-emitting diodes, Cell Reports Physical Science (2022), https://doi.org/10.1016/j.xcrp.2022.100860

for the substrate (PET/ITO/ZnO/0.8% Ag-doped CdSe/CBP/MoO_3/Al). As shown in Figure 4E, the maximum EQE and CE of device F1 are 0.086% and 0.173 cd A^{-1}, respectively. These values are higher than those of device D2, which is attributed to the fact that the substrate escape mode is enhanced in device F1 because the refractive index of PET (1.6) is higher than that of glass (1.5).[70] A photograph of device F1 under bias is shown in the Figure 4E inset. The maximum luminance of device F1 is 515 cd m^{-2}, which is lower than that of device D2. This is because the issues caused by Joule heating and layer contacting are more serious in flexible devices.[20] In addition, flexible CQW-based WLEDs have been demonstrated. With the same device architecture as device W1, except for the PET substrate, device F2 (PET/ITO/ZnO/PVK: CQWs/CBP/MoO_3/Al) has been fabricated (Figure S12). Thus, the findings pave the way for CQW-LEDs toward the field of flexible electronics.

In summary, the EL effect of noble metal dopants in NCs has been comprehensively studied by using Ag-doped CdSe CQWs. With 0.8% Ag-doped concentration, our LED device exhibits a maximum luminance of 1,339 cd m^{-2}, overtaking previous NC-based LEDs with impurity emissions as well as core-only-based CQW-LEDs. By understanding the energy gap engineering, we demonstrate the management of excitonic and dopant-induced emissions. Moreover, different HTLs possessing energies near the Ag dopant states are shown to effectively tune the dopant emission from orange-red 606 nm to NIR 761 nm. Such a large emission window is unprecedentedly achieved in NC-based LEDs with the same emitters, providing a strategy to intentionally tune the EL emissions. Furthermore, an organic-inorganic hybrid WLED based on CQWs has been successfully operated exhibiting a high CRI of 82, and flexible CQW-LEDs have been realized. The findings not only present the first step to unveil the EL property of NMD-NCs, which can be extended to other noble metal impurities (e.g., gold, ytterbium), but also pave the way for NMD-NCs as a new class of electronic materials that can be further applied to other EL applications (e.g., alternating current thin-film EL device, light-emitting field-effect transistor).

EXPERIMENTAL PROCEDURES

Resource availability

Lead contact

Further information and requests for resources and materials should be directed to and will be fulfilled by the lead contact, Hilmi Volkan Demir (hvdemir@ntu.edu.sg).

Materials availability

This study did not generate new unique materials.

Data and code availability

The data supporting the findings of this study are available from the lead contact upon reasonable request.

Synthesis of Ag-doped CdSe CQWs

In the typical procedure for the synthesis of Ag-doped CdSe CQWs, 340 mg Cd myristate, 24 mg Se, and 30 mL ODE were taken in a 100-mL round bottom flask. Then, the solution was put under vacuum for degassing to remove extra volatile impurities at 95°C for 1 h. Then, we switched to the Ar and set the temperature for the reaction to 240°C. As the temperature reached 190°C, a known amount of Ag precursor was added and the temperature of the solution was decreased to 90°C with the help of a water bath. After decreasing to 90°C, the reaction was switched to vacuum to degas the solution for a few minutes and then again converted to Ar with the temperature set to 240°C. At 130°C, 120 mg Cd acetate was introduced into the solution. The

reaction was kept at 240°C for 10 min for the growth of CQWs. The reaction was terminated by the addition of 1 mL oleic acid and brought to room temperature with the use of a water bath. Thereafter, the solution was centrifuged at 6,000 rpm for 5 min. To the supernatant, ethanol was added and centrifuged at 6,000 rpm for 5 min. Then, we discarded the supernatant, and to dissolve the precipitates, the hexane was added.

PLQY measurements

The PLQY is measured with a fixed excitation wavelength of 400 nm. All of the measurements were taken for overall PLQY in full spectrum range (540–800 nm), at only excitonic emission range (450–540 nm), and at only dopant emission range (540–800 nm).

Device fabrication

ZnO solutions were spin coated onto the ITO-coated glass substrates at 2,000 rpm for 30 s and baked at 100°C for 30 min. Then, CQWs (for dual emission) or PVK:CQWs (for white emission) were deposited by spin coating at 2,000 rpm for 35 s. Afterward, the samples were transferred into a vacuum thermal evaporation chamber to deposit other organic materials and anode. Without breaking the vacuum, HTLs (CBP, mCP, TAPC, or *m*-MTDATA), MoO_3, and Al layers were thermally deposited at a base pressure of 4.0×10^{-4} Pa. The thicknesses of layers were controlled by the quartz crystal oscillators. After preparation under a nitrogen atmosphere using epoxy glue and glass slides, all of the devices were immediately encapsulated. The emission area of all of the devices is 1×1 mm^2, as defined by the overlapping area of the anode and cathode.

Device characterization

There were two ways to measure the EL spectra of CQW-LEDs. On one side, CIE coordinates and EL spectra in the visible range were recorded via a PR705 Spectra Scan spectrometer. On the other side, EL spectra of devices with invisible emissions were measured as follows: the pump laser at 355 nm used for EL measurement of LEDs was a frequency tripling of the Nd:YAG laser, with a pulse width of 0.5 ns and a repetition rate of 100 Hz. The laser beam was focused to a spot on the device through the glass substrate using a concave-plate lens (f = 50 mm). The diameter of the focused spot, which contained (1–1/e) of the power in the laser beam, was 60 μm. An automatically rotated λ/4 waveplate (WPQ05M−532, THORLABS) and polarizer (CCM1-WPBS254, THORLABS) were used to adjust the pump fluence. Then, the emission was collected via a fiber-coupled ANDOR spectrometer (monochromator: ANDOR Shamrock 303i, CCD: ANDOR iDus 401). All of the EL spectra measurements were performed at room temperature in air. By using a computer-controlled source meter, the current density-voltage-luminance properties were measured simultaneously. Because the stability of undoped LEDs is poor, we used relatively large voltage step sizes to record their EL performance. However, both large and small voltage step sizes could be used to record the performance of doped LEDs because of better stability. The architectures of developed LEDs are shown below.

- Device D1: glass/ITO/ZnO/0.48% Ag-doped CdSe CQWs/CBP/MoO_3/Al
- Device D2: glass/ITO/ZnO/0.8% Ag-doped CdSe CQWs/CBP/MoO_3/Al
- Device D3: glass/ITO/ZnO/1.1% Ag-doped CdSe CQWs/CBP/MoO_3/Al
- Device D4: glass/ITO/ZnO/0.8% Ag-doped CdSe CQWs/mCP/MoO_3/Al
- Device D5: glass/ITO/ZnO/0.8% Ag-doped CdSe CQWs/TAPC/MoO_3/Al

- Device D6: glass/ITO/ZnO/0.8% Ag-doped CdSe CQWs/m-MTDATA/MoO_3/Al
- Device W1: glass/ITO/ZnO/PVK: 0.8% Ag-doped CdSe CQWs/CBP/MoO_3/Al
- Device W2: glass/ITO/ZnO/PVK/CBP/MoO_3/Al
- Device F1: PET/ITO/ZnO/0.8% Ag-doped CdSe CQWs/CBP/MoO_3/Al
- Device F2: PET/ITO/ZnO/PVK: 0.8% Ag-doped CdSe CQWs/CBP/MoO_3/Al

SUPPLEMENTAL INFORMATION

Supplemental information can be found online at https://doi.org/10.1016/j.xcrp.2022.100860.

ACKNOWLEDGMENTS

This research is supported by the Singapore Ministry of Education Tier 1 grant MOE-RG62/20 and the Singapore Agency for Science, Technology, and Research (A*STAR) MTC program, grant no. M21J9b0085. H.V.D. gratefully acknowledges TUBA. H.S. acknowledges the support of NRF-CRP21-2018-0007 and NRF-CRP23-2019-0007. This work was supported in part by National Natural Science Foundation of China under grant no. 62104265, in part by the Science and Technology Program of Guangdong Province under grant no. 2021A0505110009, and in part by the Innovation and Technology Fund under grant no. GHP/006/20GD.

AUTHOR CONTRIBUTIONS

H.V.D. led and supervised the project. B.L. and M.S. initiated the idea. B.L., M.S., and H.V.D. wrote the manuscript. B.L. performed LED-related experiments. B.L., M.S., and S.S. discussed the emission mechanisms of devices. M.S. synthesized and designed the CQW materials. A.S., M.I., S.D., and Y.A. assisted in materials characterizations. J.Y. and C.D. helped to measure the EL emission of CQWs. L.W. and H.S. assisted in the preparation of the flexible devices. All of the authors analyzed the data, discussed the results, commented on the manuscript, and participated in manuscript revision.

DECLARATION OF INTERESTS

The authors declare no competing interests.

Received: October 28, 2021
Revised: February 21, 2022
Accepted: March 28, 2022
Published: April 19, 2022

REFERENCES

1. Won, Y.-H., Cho, O., Kim, T., Chung, D.-Y., Kim, T., Chung, H., Jang, H., Lee, J., Kim, D., and Jang, E. (2019). Highly efficient and stable InP/ZnSe/ZnS quantum dot light-emitting diodes. Nature *575*, 634–638.

2. Shen, H.B., Gao, Q., Zhang, Y.B., Lin, Y., Lin, Q.L., Li, Z.H., Chen, L., Zeng, Z.P., Li, X.G., Jia, Y., et al. (2019). Visible quantum dot light-emitting diodes with simultaneous high brightness and efficiency. Nat. Photon. *13*, 192–197.

3. Sharma, M., Delikanli, S., and Demir, H.V. (2020). Two-dimensional CdSe-based nanoplatelets: their heterostructures, doping, photophysical properties, and applications. Proc. IEEE *108*, 655–675.

4. Wang, F., Han, Y., Lim, C.S., Lu, Y.H., Wang, J., Xu, J., Chen, H.Y., Zhang, C., Hong, M.H., and Liu, X.G. (2010). Simultaneous phase and size control of upconversion nanocrystals through lanthanide doping. Nature *463*, 1061–1065.

5. Cargnello, M., Johnston-Peck, A.C., Diroll, B.T., Wong, E., Datta, B., Damodhar, D., Doan-Nguyen, V.V.T., Herzing, A.A., Kagan, C.R., and Murray, C.B. (2015). Substitutional doping in nanocrystal superlattices. Nature *524*, 450–453.

6. Liu, Z.K., Zhong, Y.X., Shafei, I., Borman, R., Jeong, S., Chen, J., Losovyj, Y., Gao, X.F., Li, N., Du, Y.P., et al. (2019). Tuning infrared plasmon resonances in doped metal-oxide nanocrystals through cation-exchange reactions. Nat. Commun. *10*, 1394.

7. Norris, D.J., Efros, A.L., and Erwin, S.C. (2008). Doped nanocrystals. Science *319*, 1776–1779.

8. Gu, M., Zhang, Q.M., and Lamon, S. (2016). Nanomaterials for optical data storage. Nat. Rev. Mater. *1*, 16070.

9. Chen, T., Reich, K.V., Kramer, N.J., Fu, H., Kortshagen, U.R., and Shklovskii, B.I. (2016). Metal-insulator transition in films of doped semiconductor nanocrystals. Nat. Mater. *15*, 299–303.

10. Yu, J.H., Kwon, S.-H., Petrasek, Z., Park, O.K., Jun, S.W., Shin, K., Choi, M., Park, Y.I., Park, K., Na, H.B., et al. (2013). High-resolution three-photon biomedical imaging using doped ZnS nanocrystals. Nat. Mater. *12*, 359–366.

11. Xin, Y., Yu, K.F., Zhang, L.T., Yang, Y.R., Yuan, H.B., Li, H.L., Wang, L.B., and Zeng, J. (2021). Copper-based plasmonic catalysis: recent advances and future perspectives. Adv. Mater. *33*, 2008145.

12. Mocatta, D., Cohen, G., Schattner, J., Millo, O., Rabani, E., and Banin, U. (2011). Heavily doped semiconductor nanocrystal quantum dots. Science *332*, 77–81.

13. Pinchetti, V., Di, Q.M., Lorenzon, M., Camellini, A., Fasoli, M., Zavelani-Rossi, M., Meinardi, F., Zhang, J.T., Crooker, S.A., and Brovelli, S. (2018). Excitonic pathway to photoinduced magnetism in colloidal nanocrystals with nonmagnetic dopants. Nat. Nanotechnol. *13*, 145–151.

14. Liu, J.W., Ma, Q.L., Huang, Z.Q., Liu, G.G., and Zhang, H. (2019). Recent progress in graphene-based noble-metal nanocomposites for electrocatalytic applications. Adv. Mater. *31*, 1800696.

15. Son, D.H., Hughes, S.M., Yin, Y.D., and Alivisatos, A.P. (2004). Cation exchange reactions-in ionic nanocrystals. Science *306*, 1009–1012.

16. Shen, Q.H., Liu, Y., Xu, J., Meng, C.G., and Liu, X.Y. (2010). Microwave induced center-doping of silver ions in aqueous CdS nanocrystals with tunable, impurity and visible emission. Chem. Commun. *46*, 5701–5703.

17. Wei, S.J., Li, A., Liu, J.-C., Li, Z., Chen, W.X., Gong, Y., Zhang, Q.H., Cheong, W.-C., Wang, Y., Zheng, L.R., et al. (2018). Direct observation of noble metal nanoparticles transforming to thermally stable single atoms. Nat. Nanotechnol. *13*, 856–861.

18. Mashford, B.S., Stevenson, M., Popovic, Z., Hamilton, C., Zhou, Z.Q., Breen, C., Steckel, J., Bulovic, V., Bawendi, M., Coe-Sullivan, S., et al. (2013). High-efficiency quantum-dot light-emitting devices with enhanced charge injection. Nat. Photon. *7*, 407–412.

19. Yuan, M.J., Quan, L.N., Comin, R., Walters, G., Sabatini, R., Voznyy, O., Hoogland, S., Zhao, Y.B., Beauregard, E.M., Kanjanaboos, P., et al. (2016). Perovskite energy funnels for efficient light-emitting diodes. Nat. Nanotechnol. *11*, 872–877.

20. Liu, X.-K., Xu, W., Bai, S., Jin, Y., Wang, J., Friend, R.H., and Gao, F. (2021). Metal halide perovskites for light-emitting diodes. Nat. Mater. *20*, 10–21.

21. Liu, J., Zhao, Q., Liu, J.-L., Wu, Y.-S., Cheng, Y., Ji, M.-W., Qian, H.-M., Hao, W.-C., Zhang, L.-J., Wei, X.-J., et al. (2015). Heterovalent-doping-enabled efficient dopant luminescence and controllable electronic impurity via a new strategy of preparing II-VI nanocrystals. Adv. Mater. *27*, 2753–2761.

22. Liu, W.Y., Lin, Q.L., Li, H.B., Wu, K.F., Robel, I., Pietryga, J.M., and Klimov, V.I. (2016). Mn^{2+}-doped lead halide perovskite nanocrystals with dual-color emission controlled by halide content. J. Am. Chem. Soc. *138*, 14954–14961.

23. Liu, B., Sharma, M., Yu, J.H., Shendre, S., Hettiarachchi, C., Sharma, A., Yeltik, A., Wang, L., Sun, H.D., Dang, C., et al. (2019). Light-emitting diodes with cu-doped colloidal quantum wells: from ultrapure green, tunable dual-emission to white light. Small *15*, 1901983.

24. Stouwdam, J.W., and Janssen, R.A.J. (2009). Electroluminescent Cu-doped CdS quantum dots. Adv. Mater. *21*, 2916–2920.

25. Khan, A.H., Dalui, A., Mukherjee, S., Segre, C.U., Sarma, D.D., and Acharya, S. (2015). Efficient solid-state light-emitting CuCdS nanocrystals synthesized in air. Angew. Chem. Int. Ed. *54*, 2643–2648.

26. Hou, S.C., Gangishetty, M.K., Quan, Q.M., and Congreve, D.N. (2018). Efficient blue and white perovskite light-emitting diodes via manganese doping. Joule *2*, 2421–2433.

27. Ithurria, S., Tessier, M.D., Mahler, B., Lobo, R., Dubertret, B., and Efros, A. (2011). Colloidal nanoplatelets with two-dimensional electronic structure. Nat. Mater. *10*, 936–941.

28. Grim, J.Q., Christodoulou, S., Di Stasio, F., Krahne, R., Cingolani, R., Manna, L., and Moreels, I. (2014). Continuous-wave biexciton lasing at room temperature using solution-processed quantum wells. Nat. Nanotechnol. *9*, 891–895.

29. Rowland, C.E., Fedin, I., Zhang, H., Gray, S.K., Govorov, A.O., Talapin, D.V., and Schaller, R.D. (2015). Picosecond energy transfer and multiexciton transfer outpaces Auger recombination in binary CdSe nanoplatelet solids. Nat. Mater. *14*, 484–489.

30. Riedinger, A., Ott, F.D., Mule, A., Mazzotti, S., Knusel, P.N., Kress, S.J.P., Prins, F., Erwin, S.C., and Norris, D.J. (2017). An intrinsic growth instability in isotropic materials leads to quasi-two-dimensional nanoplatelets. Nat. Mater. *16*, 743–748.

31. Foroutan-Barenji, S., Erdem, O., Delikanli, S., Yagci, H.B., Gheshlaghi, N., Altintas, Y., and Demir, H.V. (2021). Single-mode lasing from a single 7 nm thick monolayer of colloidal quantum wells in a monolithic microcavity. Laser Photon. Rev *15*, 2000479.

32. Gheshlaghi, N., Foroutan-Barenji, S., Erdem, O., Altintas, Y., Shabani, F., Humayun, M.H., and Demir, H.V. (2021). Self-resonant microlasers of colloidal quantum wells constructed by direct deep patterning. Nano Lett. *21*, 4598–4605.

33. Erdem, O., Foroutan, S., Gheshlaghi, N., Guzelturk, B., Altintas, Y., and Demir, H.V. (2020). Thickness-tunable self-assembled colloidal nanoplatelet films enable ultrathin optical gain media. Nano Lett. *20*, 6459–6465.

34. Altintas, Y., Liu, B., Hernandez-Martinez, P.L., Gheshlaghi, N., Shabani, F., Sharma, M., Wang, L., Sun, H.D., Mutlugun, E., and Demir, H.V. (2020). Spectrally wide-range-tunable, efficient, and bright colloidal light-emitting diodes of quasi-2D nanoplatelets enabled by engineered alloyed heterostructures. Chem. Mater. *32*, 7874–7883.

35. Ithurria, S., and Dubertret, B. (2008). Quasi 2D colloidal CdSe platelets with thicknesses controlled at the atomic level. J. Am. Chem. Soc. *130*, 16504–16505.

36. Kelestemur, Y., Guzelturk, B., Erdem, O., Olutas, M., Gungor, K., and Demir, H.V. (2016). Platelet-in-box colloidal quantum wells: CdSe/CdS@CdS Core/Crown@Shell heteronanoplatelets. Adv. Funct. Mater. *26*, 3570–3579.

37. Altintas, Y., Gungor, K., Quliyeva, U., Erdem, O., Kelestemur, Y., Mutlugun, E., Kovalenko, M.V., and Demir, H.V. (2019). Highly stable, near-unity efficiency atomically flat semiconductor nanocrystals of CdSe/ZnS hetero-nanoplatelets enabled by ZnS-shell hot-injection growth. Small *15*, 1804854.

38. Kunneman, L.T., Schins, J.M., Pedetti, S., Heuclin, H., Grozema, F.C., Houtepen, A.J., Dubertret, B., and Siebbeles, L.D.A. (2014). Nature and decay pathways of photoexcited states in CdSe and CdSe/CdS nanoplatelets. Nano Lett. *14*, 7039–7045.

39. She, C.X., Fedin, I., Dolzhnikov, D.S., Dahlberg, P.D., Engel, G.S., Schaller, R.D., and Talapin, D.V. (2015). Red, yellow, green, and blue amplified spontaneous emission and lasing using colloidal CdSe nanoplatelets. ACS Nano *9*, 9475–9485.

40. Christodoulou, S., Climente, J.I., Planelles, J., Brescia, R., Prato, M., Martin-Garcia, B., Khan, A.H., and Moreels, I. (2018). Chloride-induced thickness control in CdSe nanoplatelets. Nano Lett. *18*, 6248–6254.

41. Maskoun, J., Gheshlaghi, N., Isik, F., Delikanli, S., Erdem, O., Erdem, E.Y., and Demir, H.V. (2021). Optical microfluidic waveguides and solution lasers of colloidal semiconductor quantum wells. Adv. Mater. *33*, 2007131.

42. Taghipour, N., Delikanli, S., Shendre, S., Sak, M., Li, M., Isik, F., Tanriover, I., Guzelturk, B., Sum, T.C., and Demir, H.V. (2020). Sub-single exciton optical gain threshold in colloidal semiconductor quantum wells with gradient alloy shelling. Nat. Commun. *11*, 3305.

43. Altintas, Y., Gungor, K., Gao, Y., Sak, M., Quliyeva, U., Bappi, G., Mutlugun, E., Sargent, E.H., and Demir, H.V. (2019). Giant alloyed hot injection shells enable ultralow optical gain threshold in colloidal quantum wells. ACS Nano *13*, 10662–10670.

44. Delikanli, S., Akgul, M.Z., Murphy, J.R., Barman, B., Tsai, Y., Scrace, T., Zhang, P.Y., Bozok, B., Hernandez-Martinez, P.L., Christodoulides, J., et al. (2015). Mn^{2+}-doped CdSe/CdS core/multishell colloidal quantum wells enabling tunable carrier-dopant exchange interactions. ACS Nano *9*, 12473–12479.

45. Sharma, M., Gungor, K., Yeltik, A., Olutas, M., Guzelturk, B., Kelestemur, Y., Erdem, T., Delikanli, S., McBride, J.R., and Demir, H.V. (2017). Near-unity emitting copper-doped colloidal semiconductor quantum wells for luminescent solar concentrators. Adv. Mater. *29*, 1700821.

46. Sahu, A., Kang, M.S., Kompch, A., Notthoff, C., Wills, A.W., Deng, D., Winterer, M., Frisbie, C.D., and Norris, D.J. (2012). Electronic impurity doping in CdSe nanocrystals. Nano Lett. *12*, 2587–2594.

47. Khan, A.H., Pinchetti, V., Tanghe, I., Dang, Z.Y., Martin-Garcia, B., Hens, Z., Van Thourhout, D., Geiregat, P., Brovelli, S., and Moreels, I. (2019). Tunable and efficient red to near-infrared photoluminescence by synergistic exploitation

of core and surface silver doping of CdSe nanoplatelets. Chem. Mater. *31*, 1450–1459.

48. Dufour, M., Izquierdo, E., Livache, C., Martinez, B., Silly, M.G., Pons, T., Lhuillier, E., Delerue, C., and Ithurria, S. (2019). Doping as a strategy to tune color of 2D colloidal nanoplatelets. ACS Appl. Mater. Interfaces *11*, 10128–10134.

49. Liu, B., Delikanli, S., Gao, Y., Dede, D., Gungor, K., and Demir, H.V. (2018). Nanocrystal light-emitting diodes based on type II nanoplatelets. Nano Energy *47*, 115–122.

50. Liu, B., Altintas, Y., Wang, L., Shendre, S., Sharma, M., Sun, H.D., Mutlugun, E., and Demir, H.V. (2020). Record high external quantum efficiency of 19.2% achieved in light-emitting diodes of colloidal quantum wells enabled by hot-injection shell growth. Adv. Mater. *32*, 1905824.

51. Chen, Z.Y., Nadal, B., Mahler, B., Aubin, H., and Dubertret, B. (2014). Quasi-2D colloidal semiconductor nanoplatelets for narrow electroluminescence. Adv. Funct. Mater. *24*, 295–302.

52. Giovanella, U., Pasini, M., Lorenzon, M., Galeotti, F., Lucchi, C., Meinardi, F., Luzzati, S., Dubertret, B., and Brovelli, S. (2018). Efficient solution-processed nanoplatelet-based light-emitting diodes with high operational stability in air. Nano Lett. *18*, 3441–3448.

53. Dufour, M., Qu, J.L., Greboval, C., Methivier, C., Lhuillier, E., and Ithurria, S. (2019). Halide ligands to release strain in cadmium chalcogenide nanoplatelets and achieve high brightness. ACS Nano *13*, 5326–5334.

54. Kelestemur, Y., Shynkarenko, Y., Anni, M., Yakunin, S., De Giorgi, M.L., and Kovalenko, M.V. (2019). Colloidal CdSe quantum wells with graded shell composition for low-threshold amplified spontaneous emission and highly efficient electroluminescence. ACS Nano *13*, 13899–13909.

55. Morgan, D., and Kelley, D.F. (2018). Role of surface states in silver-doped CdSe and CdSe/CdS quantum dots. J. Phys. Chem. C *122*, 10627–10636.

56. Liu, B., Nie, H., Zhou, X.B., Hu, S.B., Luo, D.X., Gao, D.Y., Zou, J.H., Xu, M., Wang, L., Zhao, Z.J., et al. (2016). Manipulation of charge and exciton distribution based on blue aggregation-induced emission fluorophors: a novel concept to achieve high-performance hybrid white organic light-emitting diodes. Adv. Funct. Mater. *26*, 776–783.

57. Nawrot, K.C., Sharma, M., Cichy, B., Sharma, A., Delikanli, S., Samoc, M., Demir, H.V., and Nyk, M. (2022). Spectrally resolved nonlinear optical properties of doped versus undoped quasi-2D semiconductor nanocrystals: copper and silver doping provokes strong nonlinearity in colloidal CdSe nanoplatelets. ACS Photon. *9*, 256–267.

58. Kim, M., Lee, C., and Jang, J. (2014). Fabrication of highly flexible, scalable, and high-performance supercapacitors using polyaniline/reduced graphene oxide film with enhanced electrical conductivity and crystallinity. Adv. Funct. Mater. *24*, 2489–2499.

59. Luo, J.J., Wang, X.M., Li, S.R., Liu, J., Guo, Y.M., Niu, G.D., Yao, L., Fu, Y.H., Gao, L., Dong, Q.S., et al. (2018). Efficient and stable emission of warm-white light from lead-free halide double perovskites. Nature *563*, 541–545.

60. Wang, S.M., Wang, X.D., Yao, B., Zhang, B.H., Ding, J.Q., Xie, Z.Y., and Wang, L.X. (2015). Solution-processed phosphorescent organic light-emitting diodes with ultralow driving voltage and very high power efficiency. Sci. Rep. *5*, 12487.

61. Qiu, W.M., Xiao, Z.G., Roh, K.D., Noel, N.K., Shapiro, A., Heremans, P., and Rand, B.P. (2019). Mixed lead-tin halide perovskites for efficient and wavelength-tunable near-infrared light-emitting diodes. Adv. Mater. *31*, 1806105.

62. Gao, M., Richter, B., and Kirstein, S. (1997). White-light electroluminescence from self-assembled Q-CdSe/PPV multilayer structures. Adv. Mater. *9*, 802–805.

63. Yao, E.-P., Yang, Z.L., Meng, L., Sun, P.Y., Dong, S.Q., Yang, Y., and Yang, Y. (2017). High-brightness blue and white LEDs based on inorganic perovskite nanocrystals and their composites. Adv. Mater. *29*, 1606859.

64. Bae, W.K., Lim, J., Lee, D., Park, M., Lee, H., Kwak, J., Char, K., Lee, C., and Lee, S. (2014). R/G/B/natural white light thin colloidal quantum dot-based light-emitting devices. Adv. Mater. *26*, 6387–6393.

65. Liu, X.-K., Chen, Z., Qing, J., Zhang, W.-J., Wu, B., Tam, H.L., Zhu, F.R., Zhang, X.-H., and Lee, C.-S. (2015). Remanagement of singlet and triplet excitons in single-emissive-layer hybrid white organic light-emitting devices using thermally activated delayed fluorescent blue exciplex. Adv. Mater. *27*, 7079–7085.

66. Vua, H.-T., Huang, C.-Y., Yu, H.-C., and Su, Y.-K. (2018). Ultrathin PVK charge control layer for advanced manipulation of efficient giant CdSe@ZnS/ZnS quantum dot light-emitting diodes. Org. Electron. *63*, 349–354.

67. Lee, K.-H., Han, C.-Y., Kang, H.-D., Ko, H., Lee, C., Lee, J., Myoung, N., Yim, S.-Y., and Yang, H. (2015). Highly efficient, color-reproducible full-color electroluminescent devices based on red/green/blue quantum dot-mixed multilayer. ACS Nano *9*, 10941–10949.

68. Chin, P.T.K., Hikmet, R.A.M., and Janssen, R.A.J. (2008). Energy transfer in hybrid quantum dot light-emitting diodes. J. Appl. Phys. *104*, 013108.

69. Tong, Y., Yao, E.-P., Manzi, A., Bladt, E., Wang, K., Doblinger, M., Bals, S., Muller-Buschbaum, P., Urban, A.S., Polavarapu, L., et al. (2018). Spontaneous self-assembly of perovskite nanocrystals into electronically coupled supercrystals: toward filling the green gap. Adv. Mater. *30*, 1801117.

70. Reineke, S., Lindner, F., Schwartz, G., Seidler, N., Walzer, K., Lussem, B., and Leo, K. (2009). White organic light-emitting diodes with fluorescent tube efficiency. Nature *459*, 234–238.

Cell Reports Physical Science, Volume *3*

Supplemental information

Management of electroluminescence from silver-doped colloidal quantum well light-emitting diodes

Baiquan Liu, Manoj Sharma, Junhong Yu, Lin Wang, Sushant Shendre, Ashma Sharma, Merve Izmir, Savas Delikanli, Yemliha Altintas, Cuong Dang, Handong Sun, and Hilmi Volkan Demir

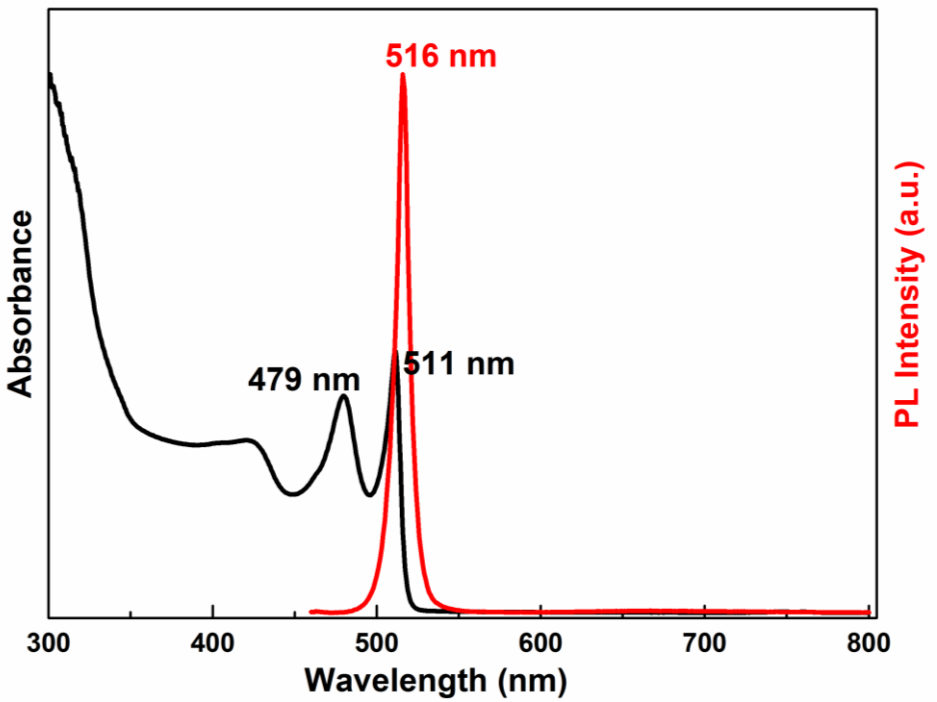

Figure S1. Absorbance and PL spectra of undoped 4ML CdSe CQWs, where only single PL emission of 516 nm is exhibited.

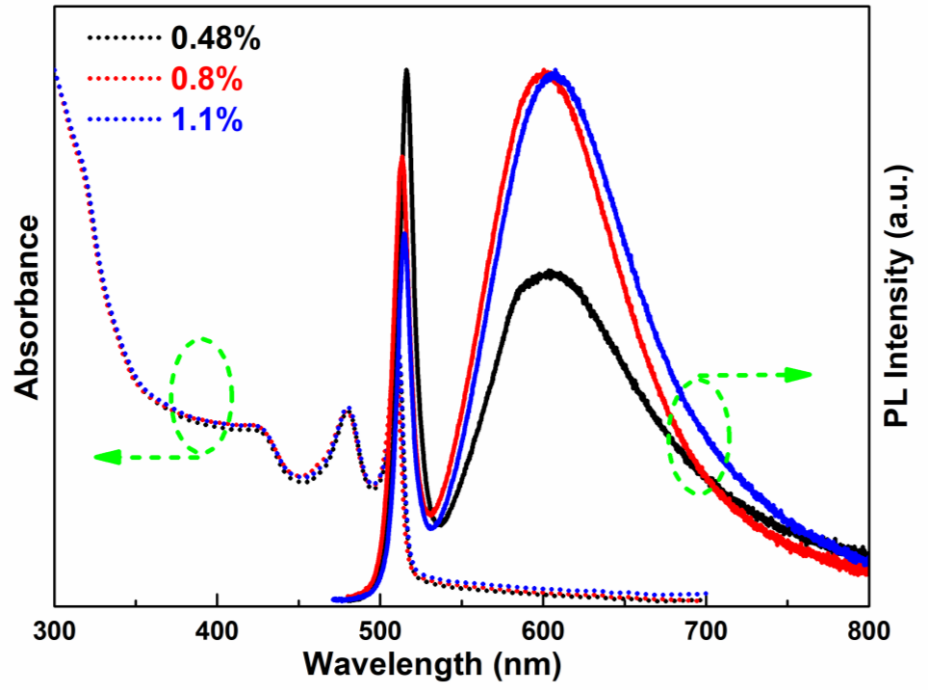

Figure S2. Absorbance and PL spectra of CdSe CQWs with 0.48%, 0.8% and 1.1% Ag-doped concentration.

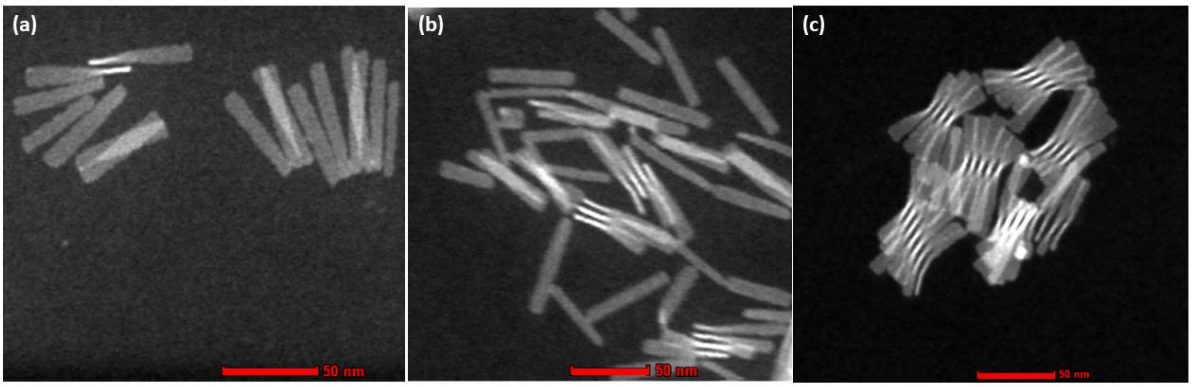

Figure S3. HAADF-STEM images of 0.48% (a), 0.8% (b), and 1.1 % (c) Ag-doped 4 ML CdSe CQWs. All of scale bars are 50 nm. Actually, doping does not change too much for the TEM dimensions. For example, the average dimensions of 0.48% and 0.8% Ag-doped CQWs are 55×7 nm^2 and 56×6 nm^2, respectively. All samples have rectangular dimensions and high aspect ratio (length/breadth around 6 to 8). Also, CQWs twist from corners and centre because of higher aspect ratio and ultrathin thickness.

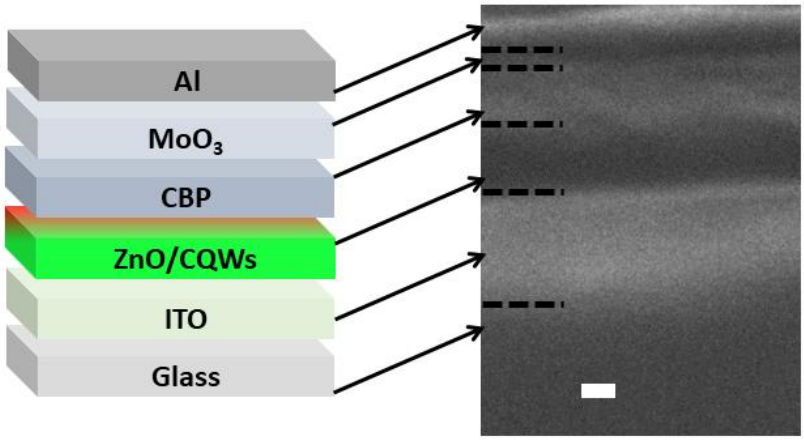

Figure S4. SEM image of Device D2. Scale bar, 100 nm. ZnO and CQWs are indistinguishable between each other because both of them are inorganic layers showing a similar contrast under SEM. The thicknesses of ZnO/CQWs, CBP and MoO_3 are about 110, 100 and 10 nm, respectively.

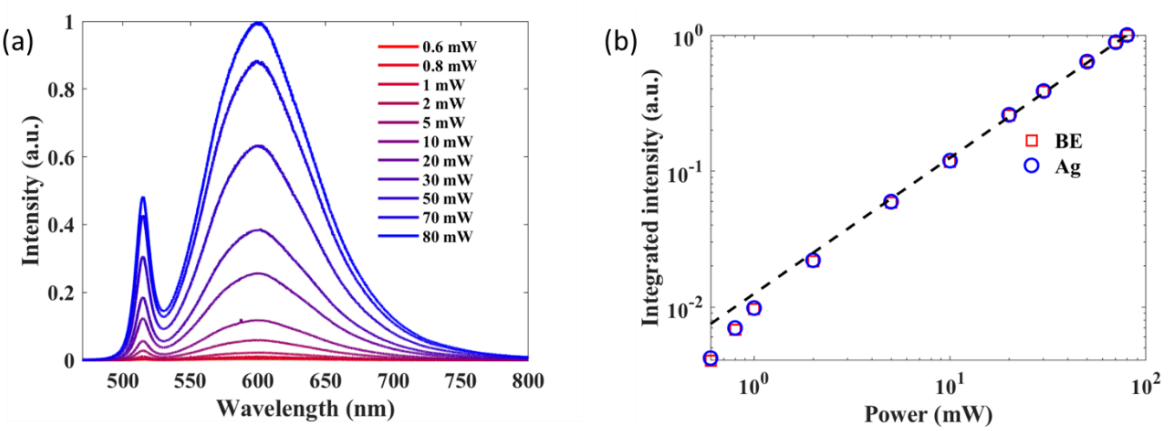

Figure S5. Power dependent PL study of Ag-doped CdSe CQWs. (a) The emission spectra as a function of the laser pumping power (laser source: continuous-wave excitation, 400 nm). (b) The linear increase relationship between the emission intensity and the pumping power. BE is band edge and Ag is Ag-dopant induced emission.

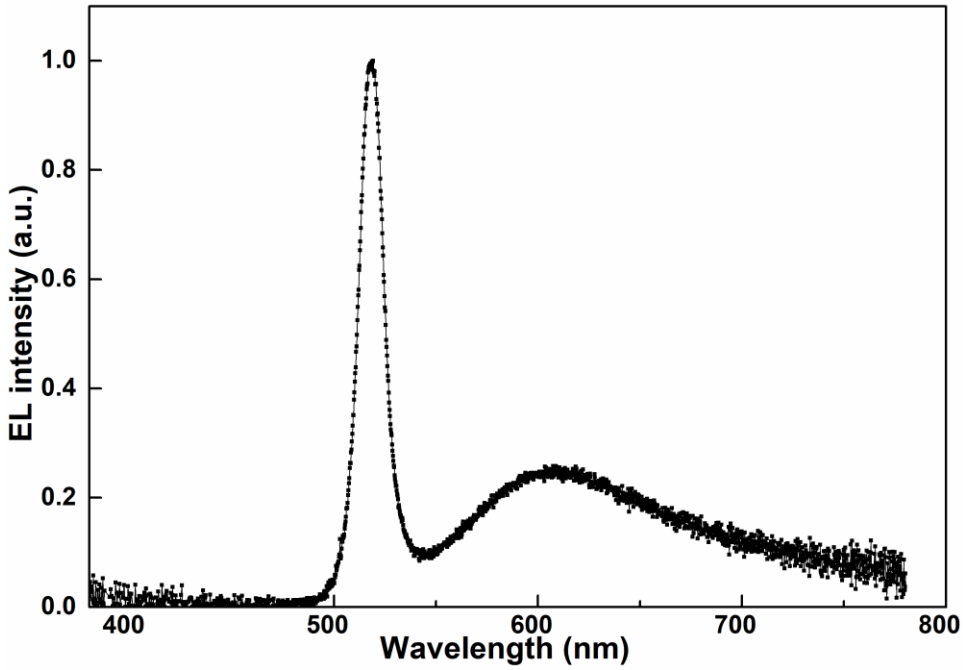

Figure S6. EL spectrum of Device D4.

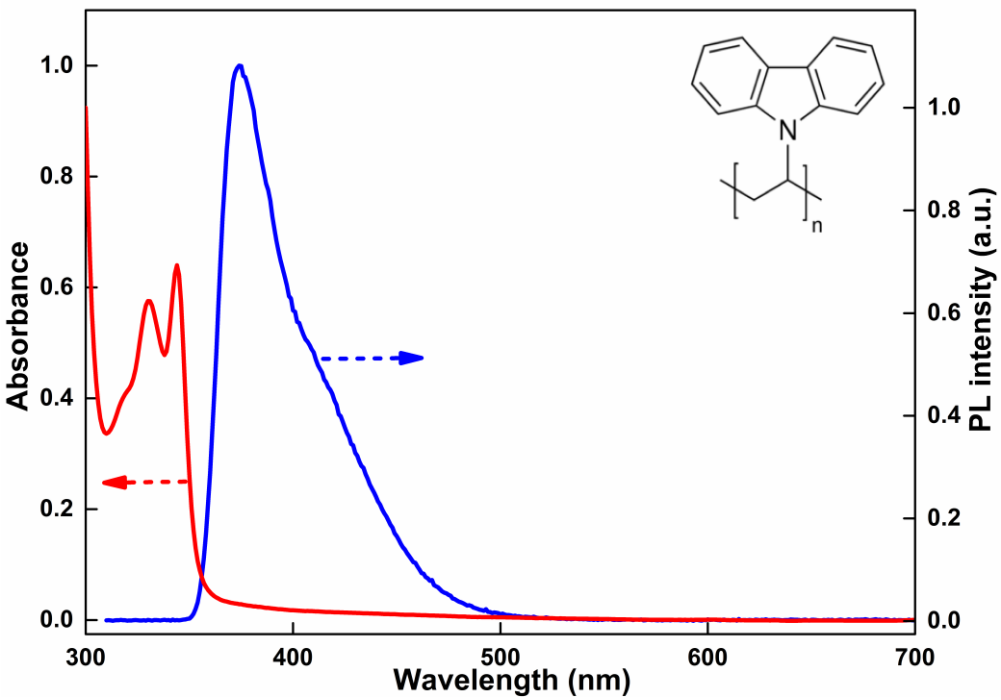

Figure S7. Absorbance and PL spectra of PVK. Inset: the chemical structure of PVK.

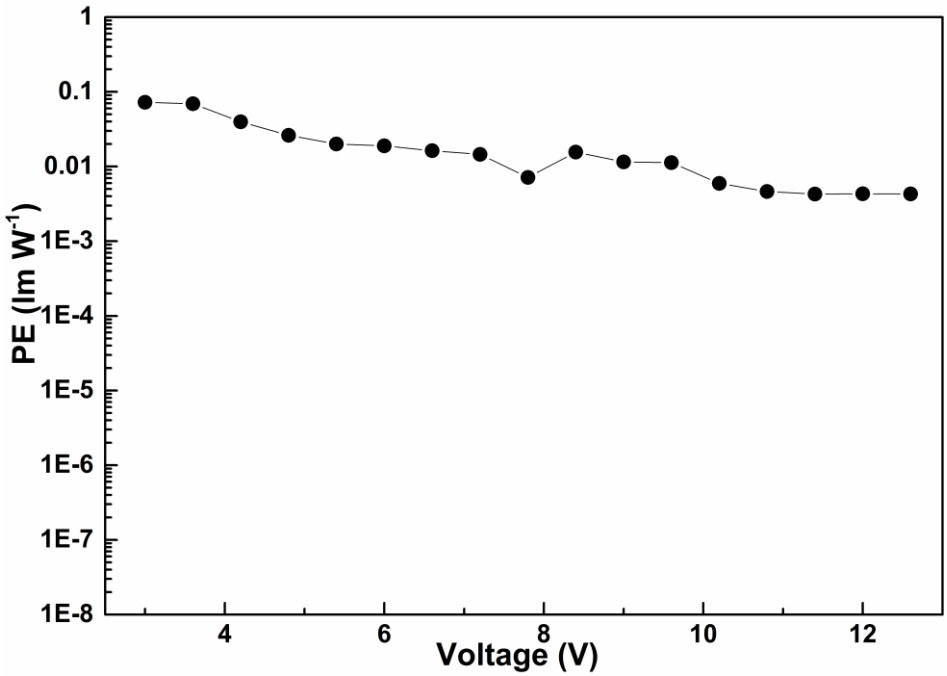

Figure S8. The PE of Device W1.

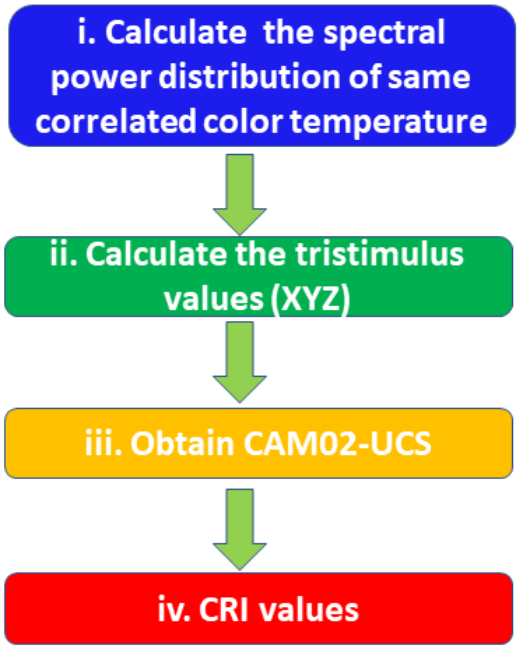

Figure S9. The simplified workflow of calculating CRI values. For white LEDs, CRI is an essential parameter for practical application of solid-state lighting, since CRI gives an indication of how well the light source will render colors of objects it illuminates. The CRI value of white LEDs is ranged from 0 to 100, which is a quantitative contrast to the ideal or natural light. For example, incandescent light bulbs have a CRI of 100, as does the sunlight. To calculate the CRI values, we adopted the CIECAM02 color appearance model, which can predict the color rendering characteristics of light sources based on the color difference between test samples illuminated under the test source and the reference illuminant.[1,2] Typically, four steps are included in this model: i) calculating the spectral power distribution of the reference illuminant possessing equal correlated color temperature as the test illuminant; ii) calculating the tristimulus values (XYZ) using 8 CIE samples defined from spectral reflectance under the test and reference illuminants; iii) obtaining CAM02-UCS through the below equation:

$$\mathrm{CAM02-UCS} = \frac{1}{8}\sum_{i=1}^{8}\left(100 - 8.0 \triangle E_{i_{\mathrm{CAM02-UCS}}}\right)$$

where 8.0 is the scaling factor, $\triangle E_{i_{\mathrm{CAM02-UCS}}}$ is the color difference for the i-th test sample; iv) calculating CRI. More details (e.g., the full CRI-CAM02UCS) for the calculation of CRI values can be found in the previous study.[1]

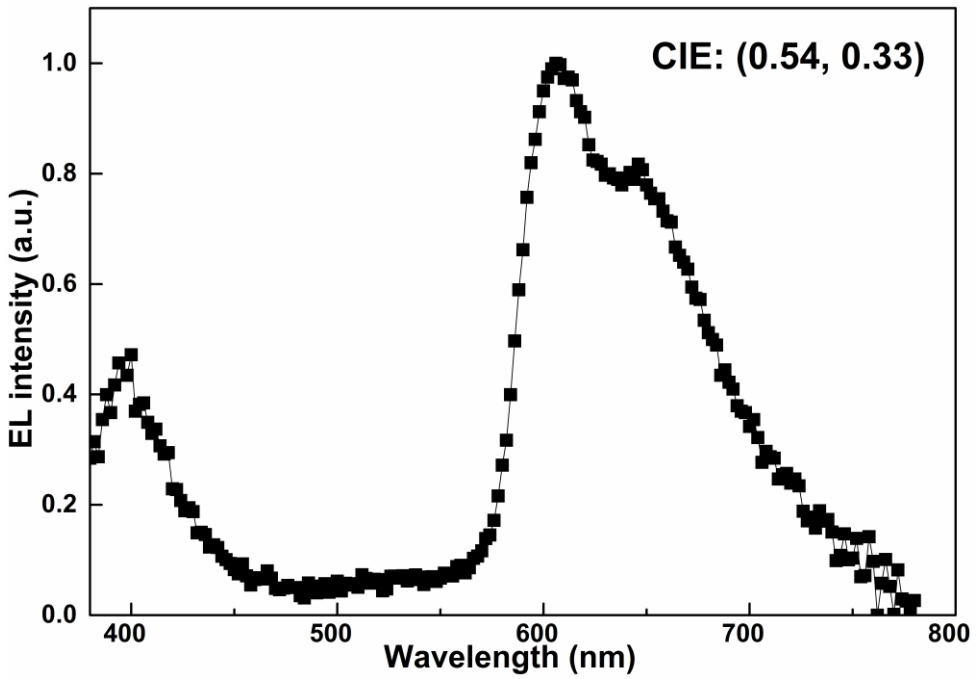

Figure S10. The EL spectrum of Device W2 at 8 V. Three emission peaks (400, 606 and 646 nm) exist in the EL spectrum, where 400 nm is originated from the blue emitter PVK and other two peaks are resulted from the interface emission.

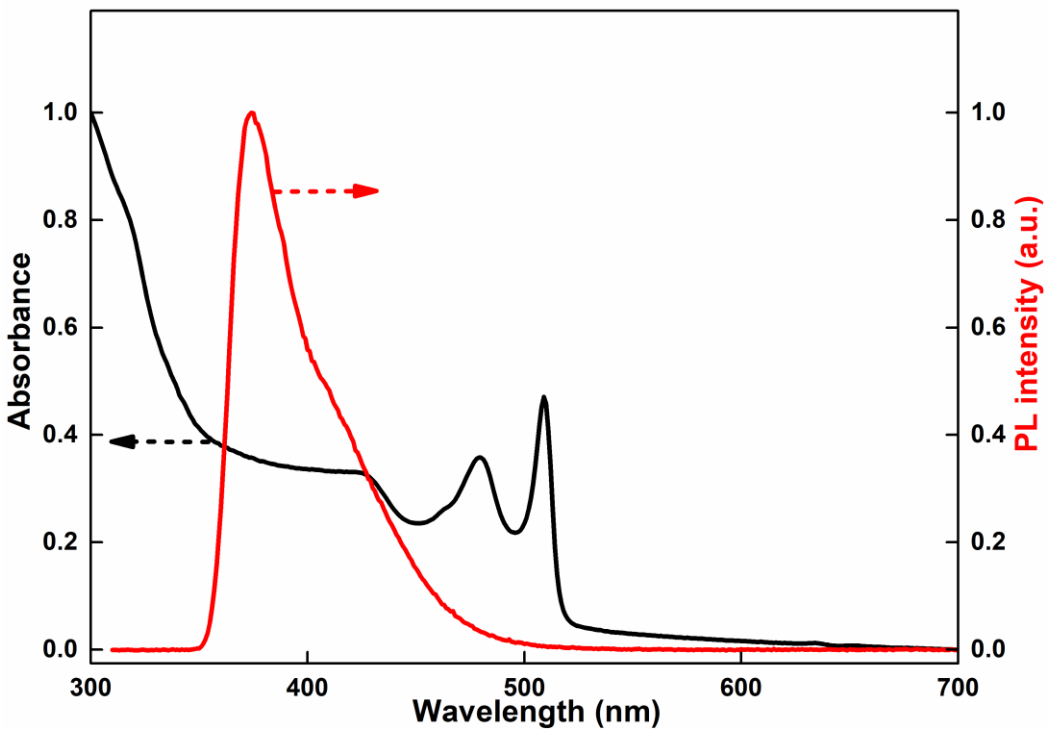

Figure S11. The absorbance of 0.8% Ag-doped CdSe CQWs and PL spectra of PVK.

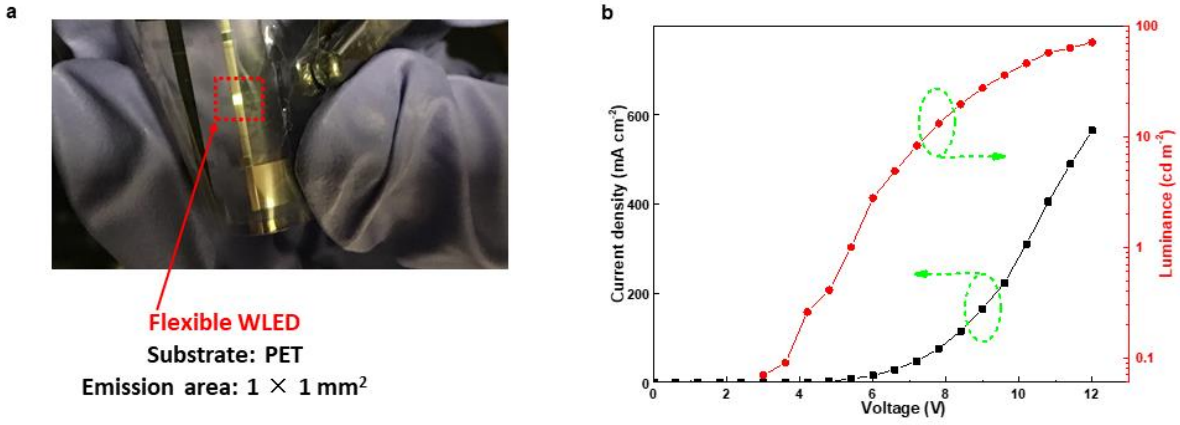

Figure S12. (a) Photograph of Device F2, in which white emission can be clearly observed. (b) Current density and luminance of Device F2, where the maximum luminance is 71 cd m^{-2}.

SUPPLEMENTAL REFERENCES

(1) Li, C., Luo, M. R., Li, C., and Cui, G. (2012). The CRI-CAM02UCS colour rendering index. Color Res. Appl. *37*, 160-167.

(2) Khan, A., Zeb, A., Li, L., Zhang, W., Sun, Z., Wang, Y., and Luo. J. (2018). A lead-free semiconducting hybrid with ultra-high color rendering index white-light emission. J. Mater. Chem. C *6*, 2801-2805.